REPORT DOCUMENTATION PAGE

Form Approved
OMB No. 0704-0188

1. REPORT DATE *(DD-MM-YYYY)*	2. REPORT TYPE	3. DATES COVERED *(From - To)*
01/09/2007	Final	06/01/2004-08/31/2006

4. TITLE AND SUBTITLE
Fuel Powered Artificial Muscles for the Robotic Soldier

5a. CONTRACT NUMBER

5b. GRANT NUMBER
W911NF-04-1-0174

5c. PROGRAM ELEMENT NUMBER

6. AUTHOR(S)
Dr. Ray Baughman

5d. PROJECT NUMBER

5e. TASK NUMBER

5f. WORK UNIT NUMBER

7. PERFORMING ORGANIZATION NAME(S) AND ADDRESS(ES)

The University of Texas at Dallas
2601 North Floyd Road, MP15
Richardson, TX 75252

8. PERFORMING ORGANIZATION REPORT NUMBER

9. SPONSORING / MONITORING AGENCY NAME(S) AND ADDRESS(ES)
US Army RDECOM
ACQ CTR – W911NF
4300 S. Miami Blvd.
Durham, NC 27703

10. SPONSOR/MONITOR'S ACRONYM(S)
US Army RDECOM

11. SPONSOR/MONITOR'S REPORT NUMBER(S)
47057.1-EG-DRP

12. DISTRIBUTION / AVAILABILITY STATEMENT

Approved for public release; unlimited distribution

13. SUPPLEMENTARY NOTES

14. ABSTRACT

15. SUBJECT TERMS

16. SECURITY CLASSIFICATION OF:			17. LIMITATION OF ABSTRACT	18. NUMBER OF PAGES	19a. NAME OF RESPONSIBLE PERSON
a. REPORT	b. ABSTRACT	c. THIS PAGE		25	Dr. Ray Baughman
					19b. TELEPHONE NUMBER *(include area code)* 972-883-6530

Final progress report for
AMSRD-ARL-RO-OI Proposal Number: 47057-EG-DRP

Fuel-Powered Artificial Muscles For The Robotic Soldier

Submitted By
The University of Texas at Dallas
Office of Research Administration and Sponsored Projects
P.O. Box 830688 MP 15
Richardson, TX 75083-0688

Submitted To:

Dr. John A. Main
DARPA/DSO, ATTN: BAA04-012
3701 North Fairfax Drive
Arlington, VA 22203-1714

and

Gary L. Anderson
Program Manager
Department of the Army
US Army Res., Dev., and Eng. Command
Army Research Office
P.O. Box 12211
Research Triangle Park
NC 27709-2211

TABLE OF CONTENTS

EXECUTIVE SUMMARY 3

CARBON NANOTUBE FUEL CELL MUSCLES 4

SHAPE MEMORY ALLOY FUEL POWERED MUSCLES 7

THERMAL IMAGING OF FUEL POWERED MUSCLES 12

DEMONSTRATIONS OF FUEL POWERED MUSCLES 13

"MERGED CONCEPT" FUEL POWERED MUSCLES 15

ELECTROCHEMICAL ACTUATION OF CARBON NANOTUBE YARNS 17

PUBLICATIONS 23

REFERENCES 24

Executive Summary

While nature's choice is to chemically power the diverse muscles of her design with a high energy density fuel, human kind has largely taken another route. Electrical energy is typically converted to mechanical energy using motors, hydraulic systems, piezoelectric, electrostrictive, or electrochemical actuators. Because of high electrical power needs, some of the most athletically capable robots cannot freely operate, since they are wired to a stationary power source. There are exceptions to this use of electrically powered actuators – chemically powered artificial muscles based on gels were demonstrated over fifty years ago and remain of practical interest for both chemically and electrically powered actuators. While actuator strains can be very large, practical utilization has been limited by low response rates, low stress generation capabilities, and the low energy densities of utilized fuels. Catalytic combustion of fuels in a pre-burner has been used to indirectly power actuation of shape-memory alloys, and muscles that act as fuel cells have been proposed, but not experimentally demonstrated.

Two types of novel actuators that are powered by high-energy-density fuels (hydrogen, methanol, or formic acid fuel combined with air or oxygen) have been experimentally demonstrated in this program. The first type uses a carbon nanotube electrode that simultaneously functions as a muscle, a fuel cell electrode and a supercapacitor electrode. The result is a muscle that converts the chemical energy in the fuel to electrical energy, and can use this electrical energy for actuation, store it, or potentially use it for other energy needs of a more complex system. The second type functions as a shorted fuel cell comprising a shape memory alloy, in which the chemical energy in a fuel converts to thermal energy that powers actuation. While the second type of fuel cell muscle provides the most powerful demonstration of the importance of this technology, the first type of fuel cell muscle provides a broader indication of technology scope. Our highest demonstrated actuator stroke and power densities for fuel cell muscles are comparable to natural skeletal muscle, and the generated stresses are over a hundred times higher than for natural muscle. Important information on temperature distribution in the muscles powered by methanol vapor/air mixture was obtained using thermal (infrared) imaging.

The concept of fuel-powered muscles was implemented in several simple demonstrations ("robotic arm", "weight lifting", etc) that were created to illustrate performance gain and potential applications of the fuel-powered devices. The demonstrations featured in broadcasts of a number of TV news channels (Fox News, ABC News, CNN), scientific channels (Discovery-Canada, Science-Korea) and numerous Internet sites. Also, the fuel cell muscles developed in this program have been reported in the *New York Times*, the *Dallas Business Journal*, the *Dallas Morning News*, *La Monde* (France), the *Guardian* (UK), the *New Scientist*, *Discovery Channel News*, the *Observer* (UK), *Electronics Design Magazine*, *Science News*, BBC News, and many more places here and abroad. Similar high impact coverage resulted from our program-funded reports in

Science of methods for the fabrication of nanotube sheets and yarns for program use.

We also showed that properties of the two types of fuel-powered muscles can be merged to provide benefits of both. Proposed by us hybrid device combined operation of the Proton Exchange Membrane Fuel Cell (PEMFC) with the highly efficient shape memory alloy (SMA) actuation. It can be powered by high energy density fuels (hydrogen, noncombustible mixture of hydrogen in an inert gas, methanol) and can be controlled electrically or by interruption of fuel supply.

In order to control device operation, we designed, built and tested an electrochemical micro-array sensor capable of detecting methanol concentration in water. This study reported in the *Journal of Nanoscience and Nanotechnology* is aimed at use of the sensors in portable methanol-powered units.

The need for electrodes that are highly deformable in appropriate directions without interfering with the displacement of high stroke artificial muscles helped motivate our development of twist based nanotube yarns and nanotube sheets, which we reported in two papers in *Science*. Actuation of the material in response to voltage ramps and potentiostatic pulses was investigated by us in the *Journal of Smart Materials and Structures*. Strains of up to 0.5 % are obtained in response to applied potentials of 2 V. Also, our overview of the artificial muscle area in *Science* was funded by this program, as well as a paper that we published in *Science* on fuel powered artificial muscles. Our breakthrough on twist-based yarns and sheets was recognized by our receiving in Frankfurt, Germany the New Materials Innovation Prize of the Avantex International Forum for Innovative Textiles, the NanoVic Prize (Australia), a Nano50 award, and by our being listed (along with Al Gore and Warren Buffet) on the Scientific American 50 list. These papers are in the appendix.

Another output of the program is a provisional patent filing (with 215 non-trivial claims) in the United States on the solid-state fabrication of nanotube sheets and twisted yarns, which will be converted to at least five utility filings in the United States. Presently we are drafting a provisional filing in the United States on our Fuel Powered Artificial Muscles.

Carbon Nanotube Fuel Cell Muscle

Our first fabricated fuel cell muscle type is electrochemical and uses a catalyst-containing carbon nanotube sheet electrode as the actuator material. While both working and counter-electrodes can be actuating electrodes, only one electrode is used for actuation in these initial concept demonstrations. Like for the previously described electrically powered carbon nanotube artificial muscles, reversible dimensional changes result from electronic charge injection in carbon nanotubes. The simultaneous movement of ions of the electrolyte into close proximity to the injected electronic charge forms the so-called electrochemical double layer, which enables very high charge injection by largely maintaining overall charge neutrality. This close proximity of electronic charge and counter ions in the electrolyte is enabled by the nanoscale porosity of the nanotube sheets and the corresponding high surface area, above 300 m^2/gm.

Instead of actuating in response to an externally applied potential, the chemically powered actuator electrode generates this potential by acting as a fuel cell electrode. The first demonstration is for a cantilevered actuator (Figure 1a) in which a nanotube sheet strip layer is laminated with a layer comprising a mixture of Pt-coated carbon and a Nafion ionomer. The actuating cantilever electrode was immersed in 1 M H_2SO_4 and the counter electrode was a platinum-carbon paste deposited on a Nafion-117 membrane, which separated the fuel (hydrogen, at the counter electrode) from the oxidant (oxygen, at the nanotube actuator electrode) and enabled hydrogen ion diffusion between electrodes when the electrodes are shorted.

While ordinary fuel cells operate by generating electrical energy when the fuel cell electrodes are connected through a load, the present fuel cell muscle generates and capacitively stores electrical energy (and causes actuation) when the inter-electrode circuit is open. With the external circuit open, hydrogen gas at the nanotube electrode is oxidized in the presence of platinum catalysts to form protons and electrons until equilibrium is reached, generating a half-cell potential of 0.00V (versus normal hydrogen electrode, NHE) (Figure 1a). The injected electrons cause actuation of the nanotube sheet, and the protons are counter charges in the electrochemical double layer. At the opposite electrode under open circuit conditions, the reduction of oxygen generates a half-cell potential of 0.9 V (theoretically 1.22 V vs. NHE, Figure 1a). This occurs because of an overall reaction in which four protons in the H_2SO_4 combine with an O_2 and four electrons extracted from the oxygen electrode to produce two water molecules. The resulting four holes on the oxygen electrode are counterbalanced by two SO_4^{2-} ions, which form the double layer of a charged capacitor electrode. Note the difference from continuous operation of an ordinary hydrogen fuel cell, where the protons in the reaction come from the hydrogen electrode via diffusion through the electrolyte. The discharge phase of the fuel cell muscle, where the direction of actuation is reversed, corresponds to recombination of electrons on the hydrogen electrode with the holes on the oxygen electrode (the actuating nanotube sheet) and the corresponding diffusion of H_2 derived protons to the oxygen electrode to replace H^+ ions in the electrolyte that were used to make water during the charge-injection part of the actuator cycle.

The observed actuator stroke during chemically driven charge injection is a 3 mm deflection of a 3 cm long nanotube cantilever in ~5 sec while the nanotube electrode potential increases to ~0.8 V (versus NHE). The opposite actuator deflection, obtained when the hydrogen and oxygen electrodes are shorted, occurs within a second. Breaking the connection between electrodes causes recharging of the nanotube muscle and return to the deflection of the initially charged state. While these results provide important concept demonstrations, much more work is required to provide a commercially deployable technology. As will be seen below, our program-developed fuel powered muscles provide much more attractive performance, and are ready for advanced stages of productization.

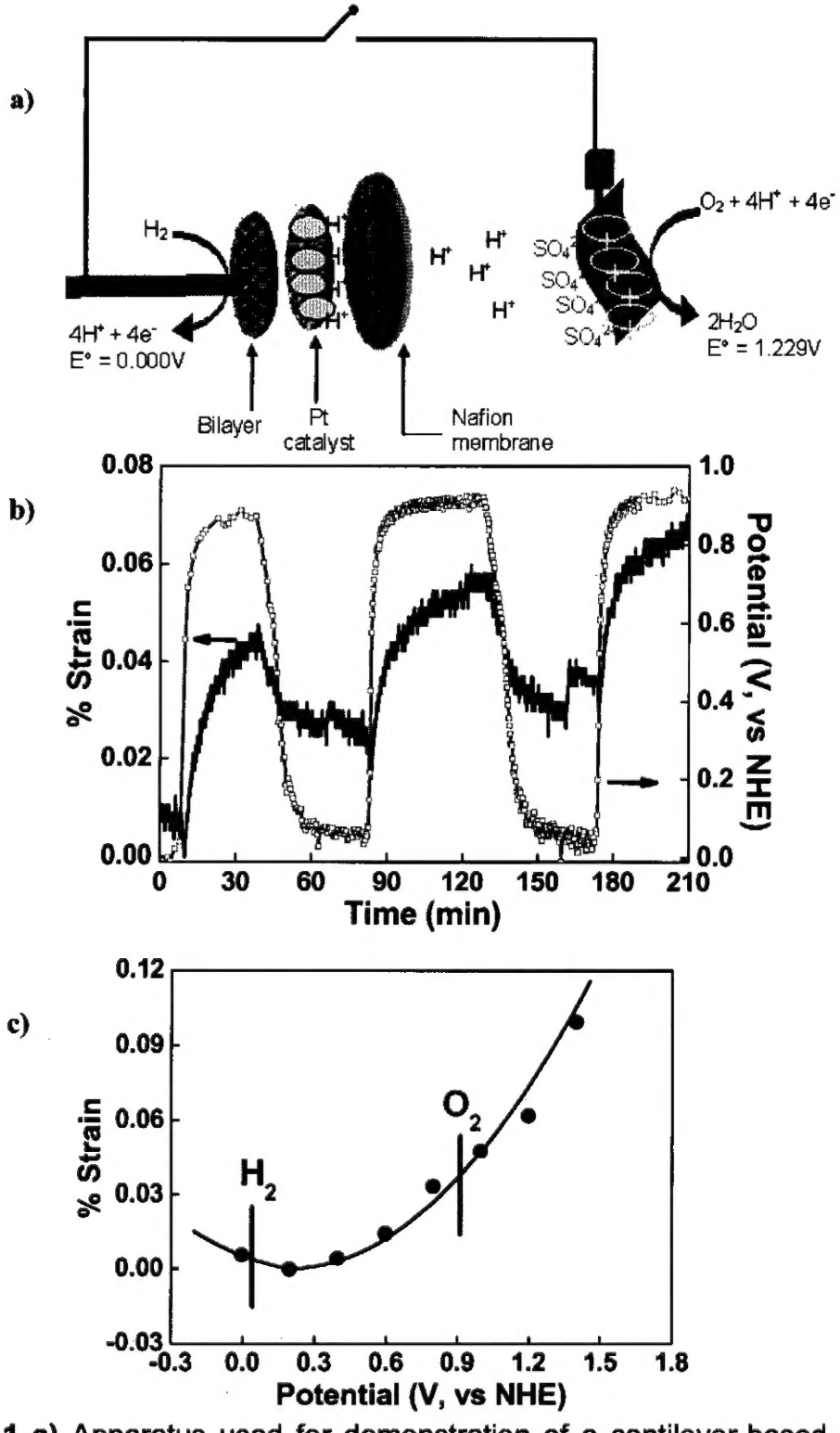

Figure 1 a) Apparatus used for demonstration of a cantilever-based nanotube fuel cell muscle. **b)** Potential and actuator strain versus time for a tensile actuator exposed to a mixture of 5 volume percent H_2 in inert gas (blue) and pure O_2 (red). **c)** Measured tensile actuator strain versus potential for an electrically powered nanotube actuator.

While this fuel cell muscle actuator uses only one electrode for actuation, it is easily shown that both electrodes could have simultaneously served as actuators. This was done by switching the oxygen and hydrogen delivery chambers, so the nanotube electrode becomes the hydrogen electrode. Other than decreasing the time required for the charge-injection stroke to 1-2 seconds and causing a 180° phase shift in actuator response direction, no change in nanotube sheet actuation was observed. This phase shift and unchanged actuation amplitude results since the charge storage and delivery capacity of the nanotube sheet electrode is much lower than for the much larger counter-electrode. Hence, shorting the electrodes brings the nanotube sheet potential to close to that of the unshorted counter-electrode. Consequently, the nanotube electrode cycles between ~0 V and ~0.8 V (versus NHE) during charge and discharge and only the direction of this shift depends upon whether the nanotube electrode is the oxygen electrode or the hydrogen electrode.

Again using hydrogen as the fuel, oxygen as the oxidant, and 1M H_2SO_4 as electrolyte, we also drove forward and reverse actuation of a Pt-containing nanotube sheet in a one compartment cell. Instead of using a cantilever type actuator as the electrode, we used a nanotube sheet that was uniformly filled with catalyst and characterized actuation in tension. In the forward actuation step, the nanotube sheet was double-layer charged to ~0 V (vs. NHE) by filling the cell with hydrogen. After purging the cell with N_2 to avoid direct contact of a H_2 and oxygen mixture with the catalyst, we filled the cell with oxygen, which reversed the charging and actuation direction as a nanotube electrode went to a potential of ~0.8 V (versus NHE). While very long actuation times result in this configuration from the need to periodically dissolve gases in relatively massive amounts of electrolyte, this experiment enables reliable comparison between chemically driven and electrically driven actuation in the same electrolyte for the same type of Pt-infiltrated nanotube sheet. The obtained results (Figure 1b) show that the potential changes from ~0.0 V to ~0.87V (vs. NHE) as the hydrogen gas in the cell is switched to oxygen, and that the length increase of the nanotube sheet is ~0.035%. Essentially the same length change results for electrically driven actuation between these potentials in the utilized electrolyte (Figure 1c).

Shape Memory Fuel Cell Muscle

This fuel cell muscle benefits from a liability of fuel cells: the efficiencies of traditional polymer electrolyte membrane fuel cells do not exceed 40%, and the remainder of this energy is converted to heat. This muscle is called a "continuously shorted fuel cell muscle" since the half-cell reactions of an ordinary fuel cell occur on the actuator material, which can be a shape memory alloy. Though the possibility of this type of muscle has been discussed, experimental demonstration has not been reported. The closest experimental demonstration has been for a system in which fuels are oxidized to produce heat in a catalytic converter device, and this heat is directed to a shape memory material – where actuation is produced.

The present first demonstration uses a NiTi alloy shape memory wire (Nitinol) coated with Pt catalyst as the fuel cell muscle and either hydrogen, methanol, or formic acid as fuel. Contact of the fuel and an oxidant (oxygen or air) causes the mechanically loaded shape memory wire to heat to above the austenite phase transition temperature (A_s) and the shape memory wire does work as it contracts (Figure 2b). Interruption of the fuel results in cooling below the martensite phase transition temperature (M_s), and the wire returns to its original length.

The above fuel powered muscle (Figure 2a) generated 150 MPa or higher stress while undergoing a 5% stroke when powered by a mixture of oxygen (or air) and either methanol vapor, formic acid vapor, or 2.5 volume percent non-combustible mixture of H_2 in inert gas. This stress generation capability is 500X that typical of human skeletal muscle (0.3 MPa), while the percent stroke is about ¼ th that typical of natural muscle. Hence, the work capability of the continuously shorted fuel cell muscle on lifting a weight (5300 kJ/m^3 for methanol fuel and formic acid fuel and 6800 kJ/m^3 for hydrogen fuel) is over a hundred times that of skeletal muscle (~40 kJ/m^3). The percent contraction (5%, 7%, and 8.0% observed for 150, 122, and 98 MPa load, respectively, using 2.5 volume percent hydrogen in inert gas as fuel) can be increased to far above the ~20% typical of skeletal muscle by simply coiling the shape memory wire – albeit with a proportional decrease of stress generation capability. The presently achieved power density (68 W/kg for hydrogen fuel) is similar to natural skeletal muscle, which is typically 50 W/kg. By increasing the delivery rate of the fuel, optimizing fuel composition, and optimizing catalyst coating, it should be possible to dramatically increase power density.

This initially obtained performance indicates those shape-memory-alloy based fuel cell actuators are quite promising for such applications as powering autonomous robots, wearable robots (exosketetons), and prosthetic limbs. Eliminating the need for separate fuel cell and electrical power conditioning equipment and harvesting the ~40% energy loss due to fuel cell heating provide advantages over conventionally conceived fuel-cell-driven electrical actuators. The high energy density of fuels like methanol (7.5 X that of advanced lithium batteries) provides an major advantage over battery powered muscles, as does the shorter time for fuel injection than for battery recharge.

Merging aspects of the capacitively and thermally activated fuel cell muscles can expand future possibilities. For example, the shape memory metal alloys could be made into catalyst-coated high-surface-area nanofiber yarns or nanoparticle compactions that function in an electrolyte as a fuel-charged capacitor. Like for the nanotube muscles and metal-based muscles of other types, charge injection will cause small actuator strokes (typically 0.1 % or less, as for high modulus ferroelectric actuators).

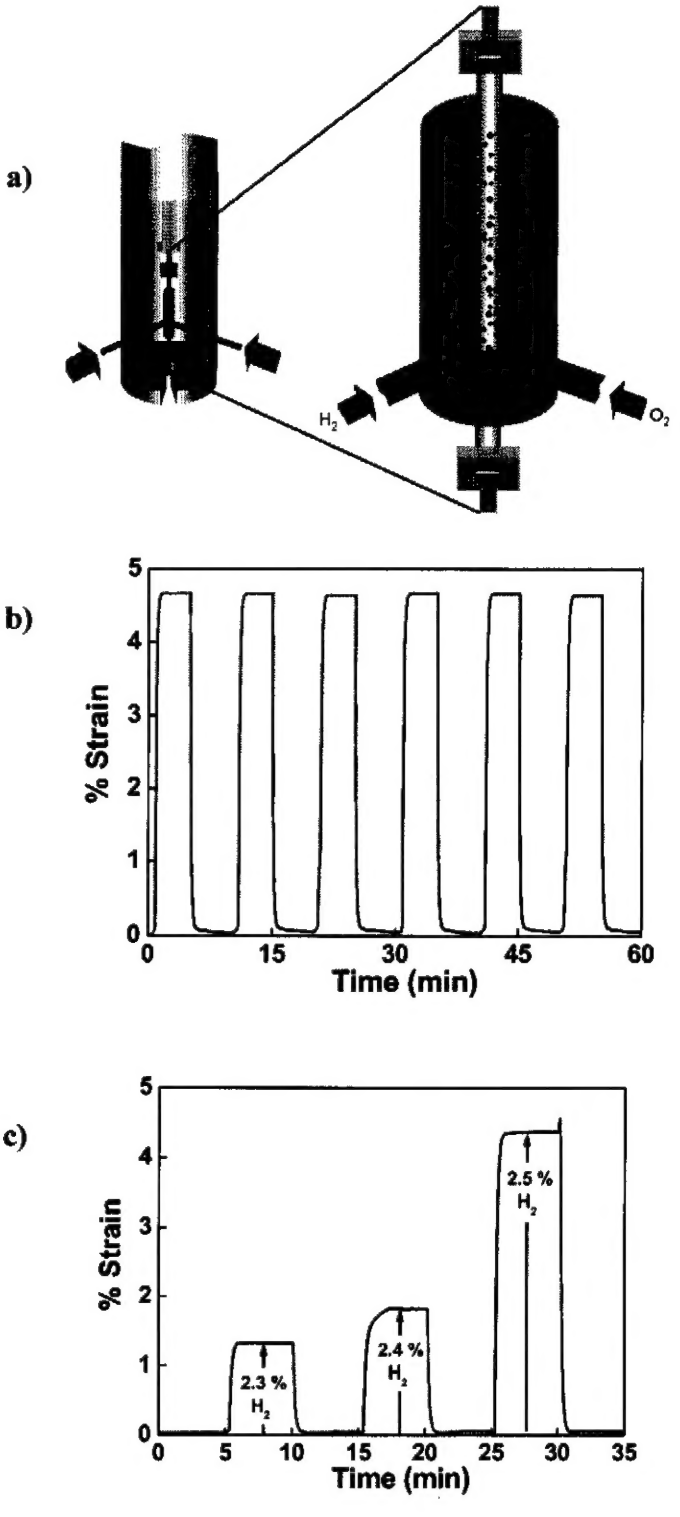

Figure 2. **a)** A simplified illustration of the fuel-powered artificial muscle mounted in the measurement device. **b)** Actuator strain versus time during exposure to a mixture of 2.5 vol % H_2 and 50 vol % O_2 (red curves), while exposure to pure oxygen (blue lines). **c)** Actuator strain versus time for the experiment in b, where the volume percent of hydrogen is varied.

The energy of capacitor discharge can be used to either heat the shape memory electrodes to above the shape memory transition (thereby causing relatively giant stroke actuation), to power other energy-requiring systems, or both. The major advantage of this merged concept muscle is that actuator switching can be accomplished by electrical switching without the need to interrupt or switch fuel feed or the use of an external power source.

The demonstrated concept of chemically powered thermal actuation is more generically applicable to other than shape memory alloys. It will work for the commonly utilized thermal-expansion-based cantilevers in MEMs (MicroElectroMechanical) devices, by simply replacing electrical heating by catalyst-mediated chemically-produced heating. Likewise, the heating produced by a high-energy-density fuel can be used to power actuation of either other known shape memory compositions or other known materials whose volumetric transitions can do mechanical work in hydraulic systems.

Additional experiments, not pertinent to the main text, were conducted using the shape memory alloys (SMAs). The bulk of them were centered around the placement of Pt on the wire to create a SMA fuel cell muscle that was robust and had the desired catalytic activity. This was achieved in a variety of ways. Each offered potential benefits and problems. The goal was to attach a maximum amount of Pt to the surface of the SMA wire, while providing accessible surface area for gas diffusion.

Catalyst Attachment

A thin coating stopcock grease was applied to the SMA wire, and then the wire was dragged through a dry Pt source. This allowed large amounts of catalyst to be attached in a reasonably robust fashion. Problems arose when the actuating wire was actuated over many cycled. The grease could soften and coat the catalyst. This caused loss of catalyst activity and ultimately to total failure of the devices.

Conventional electroplating was also employed for connecting the catalyst onto the shape memory wire. The resultant wire did not deliver any useable actuation when exposed to hydrogen and oxygen, likely because of the large size of the deposited Pt. This is an area of future investigation that may yield usable materials.

The simplest and most reliable deposition method relied on liquid delivery to attach the particles onto the wire. The catalyst was combined with an organic solvent (i.e. hexanes) and the wire was buried in the catalyst. After the solvent evaporated the catalyst clumped onto the wire. The wire was then hit with a stream of compress air to knock off excess catalyst. This process typically deposited 1.3-1.5% wt Pt onto the wire. This was sufficient to allow the desired fuel cell reactions (at below 2.5% H_2 in O_2 and inert gas) for numerous (>20) cycles. This attachment method was suitable regardless of the fuel, as long as fuel combustion could be catalyzed by the Pt. A thermocouple was exposed coated with catalyst in the same fashion, then exposed to the 2.5% of H_2 in O_2 and inert gas while temperature was monitored (Figure 3). This was attempted with methanol also, but this experiment resulted in rapid temperature increase

(>800°C in less than 30s), starting a minor fire. This method was not attempted with formic acid.

Another potentially useful method of catalyst attachment was by incorporating catalytic metal into the alloy matrix of a SMA, and then leaching the non-catalytic component from surface of the SMA. The investigated alloy ($Pd_2Ni_3Ti_5$) was obtained from Texas A&M (SMART Lab). This alloy's transition temperature was 450°C. The sample was placed in sulfuric acid and anodically stripped at 8V and 1A for 30 minutes. The stripping left a majority of the surface covered with Pd metal (oxidation potential -0.960V) and eroding the Ni and Ti (oxidation potentials 0.257 and 0.860V respectively). The resultant material was wrapped by a temperature probe and temperature was monitored during gas exposure. While the observed 6°C jump in temperature is too small to be useful, this approach deserves further evaluation in our continuing work.

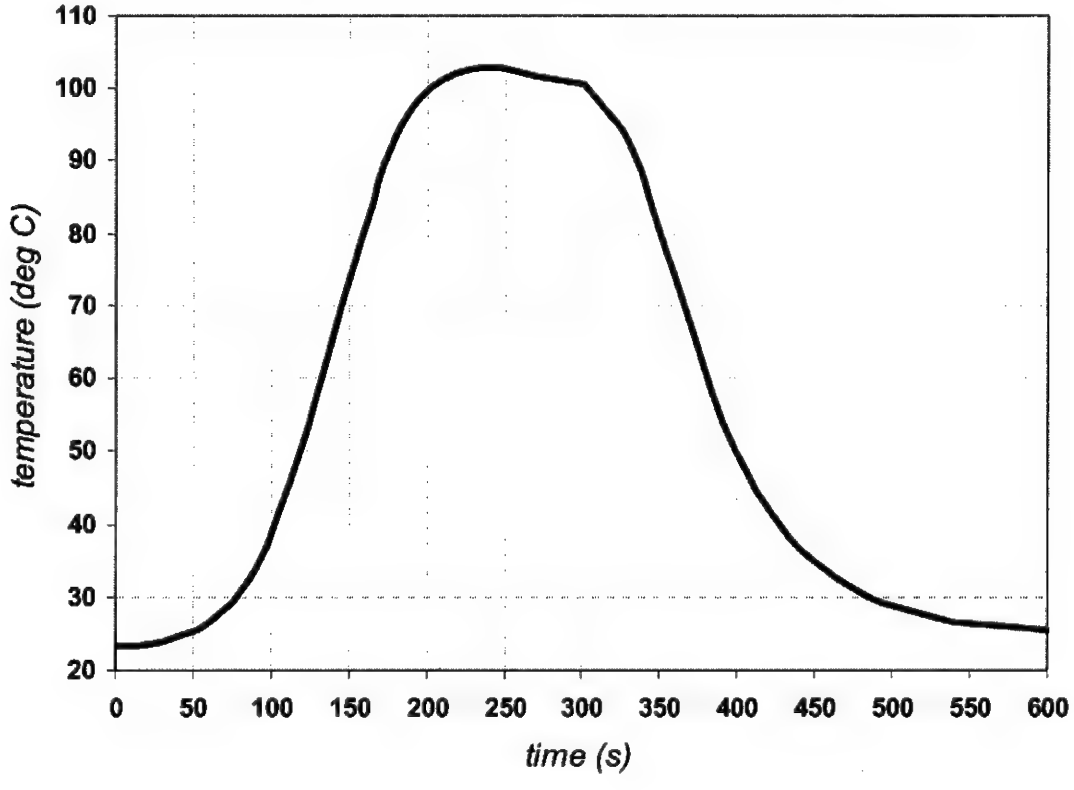

Figure 3 Time vs. temperature plot for a temperature probe that was coated with Pt-black by submerging in a slurry made from hexanes. Blue line segments indicate exposure to a H_2/O_2 mix (2.5 vol. % H_2 and 50 vol. % O_2), while red line segments indicate exposure to only O_2.

Merging aspects of the capacitively and thermally activated fuel cell muscles can expand future possibilities. For example, the shape memory metal alloys could be made into catalyst-containing, high-surface-area metal nanofiber yarns that function in an electrolyte as electrodes of a fuel-charged capacitor. Charge injection will cause small-stroke actuation of the capacitor electrodes and

the energy of capacitor discharge can be used to either power large-stroke shape memory actuation, other energy-requiring systems, or both. The major advantage of this merged concept muscle over the continuously shorted fuel cell is that actuator switching can be accomplished by opening or closing a circuit without the need to interrupt or switch fuel feed. A tunable muscle compliance is needed for ordinary robotic tasks, and a fuel driven transition between the high modulus martensitic phase and the much lower modulus austenitic phase of a shape memory alloy could provide this.

The demonstrated fuel-powered actuation methods could be extended to other actuator materials and systems, like shape memory polymers and polymer composites, solids with large volume changes that do work in hydraulic systems and thermal-expansion-based cantilevers in microelectromechanical systems (MEMS). By replacing metal catalyst with tethered enzymes, it might eventually be possible to use artificial muscles powered by food-derived fuels for actuation in the human body.

Thermal Imaging of Fuel-powered Muscles

Important information on temperature distribution in carbon nanotube-based and shape memory alloy (SMA)-based artificial muscles powered by methanol vapor/air mixture can be obtained using thermal imaging often referred as to thermography. Thermography is the use of an infrared imaging and measurement camera to "see" and "measure" thermal energy emitted from an

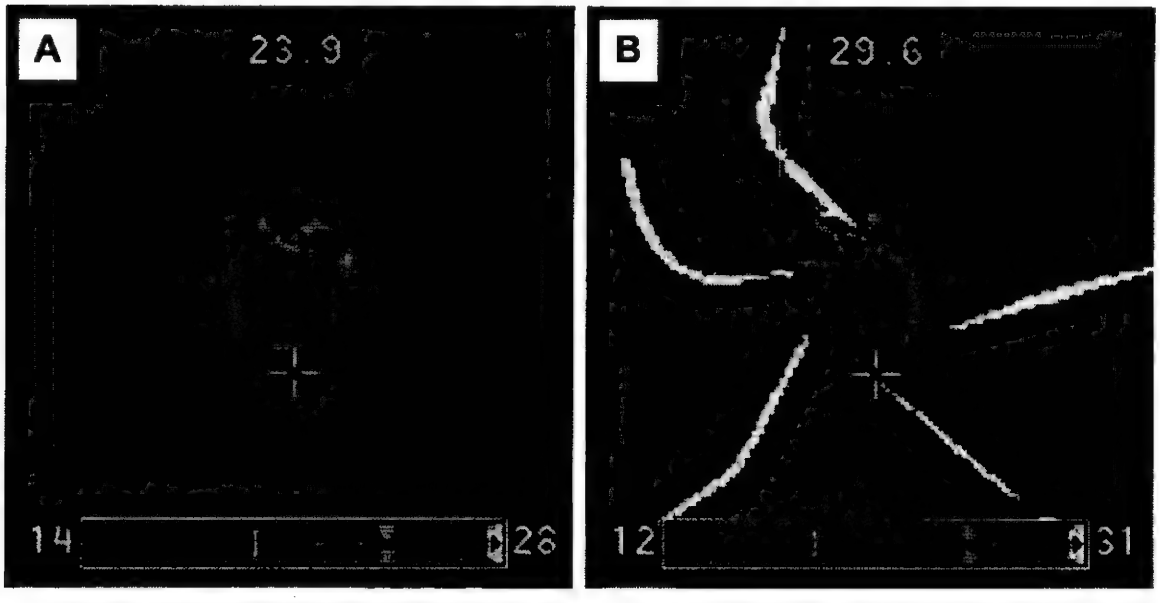

Figure 4. Thermal (infrared) image of a complex shape-memory ribbon structure coated with Pt particles before (A) and after (B) exposure to methanol vapor/air mixture. Increase in temperature from 29.1° C to 127° C can be clearly seen, and correlated with shape changes in the shape arms, which are radial to the central hub.

object. Infrared thermography cameras produce images of invisible infrared or "heat" radiation and provide precise non-contact temperature measurement capabilities.

Thermal images recorded with Raz-IR infrared camera during shape-memory actuation are shown in Figures 4. They were obtained using uncooled FPA microbolometer, with image correction and instant image enhancement. The camera covers Long Wave Infrared (LWIR) spectral range 8-14μm.

Demonstrations of Fuel Powered Muscles

Application opportunities of our fuel powered shape-memory muscles are diverse, and range from robots and morphing air vehicles to dynamic Braille displays and muscles powered by the fuel/air mixture delivered to an engine that is able to regulate this mixture. The more than 30 times higher energy density obtainable for fuels like methanol, compared to that for the most advanced batteries, can translate into long operational lifetimes without refueling for autonomous robots. This refueling requires negligible time compared with that needed for recharging batteries.

The fuel-powered muscles can be easily downsized to the micro- and nano-scales, and arrays of such micro-muscles could be used in "smart skins" that improve the performance of marine and aerospace vehicles. By replacing metal catalyst with tethered enzymes, it might eventually be possible to use artificial muscles powered by food-derived fuels for actuation in the human body – perhaps even for artificial hearts.

In order to illustrate potential applications of the fuel-powered muscles we created several simple "concept demonstrations". These demonstrations featured in broadcasts of a number of TV news channels and numerous Internet sites. They are available in the form of digitally recorded real-time movies.

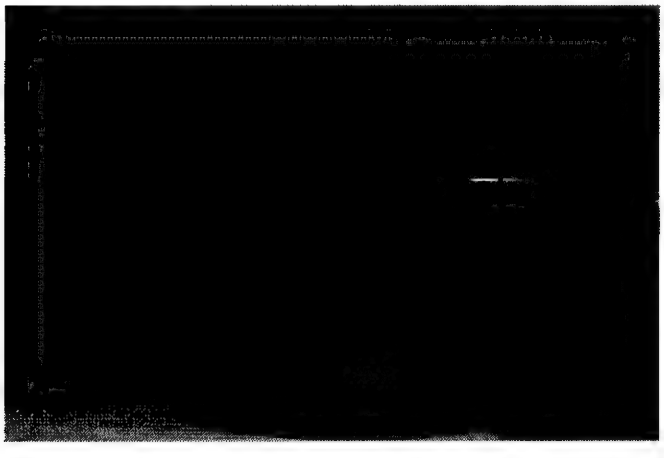

Figure 5. A miniature robot arm "surfing" on the methanol/air mixture above a dish of methanol. The arm rises when the invisible Pt-coated nickel-titanium shape memory wire is heated by the fuel to above the shape memory transition temperature. This upwards motion brings the fuel-powered wire to a position where there is less fuel, and the resulting cooling (and expansion) of the wire lowers the arm.

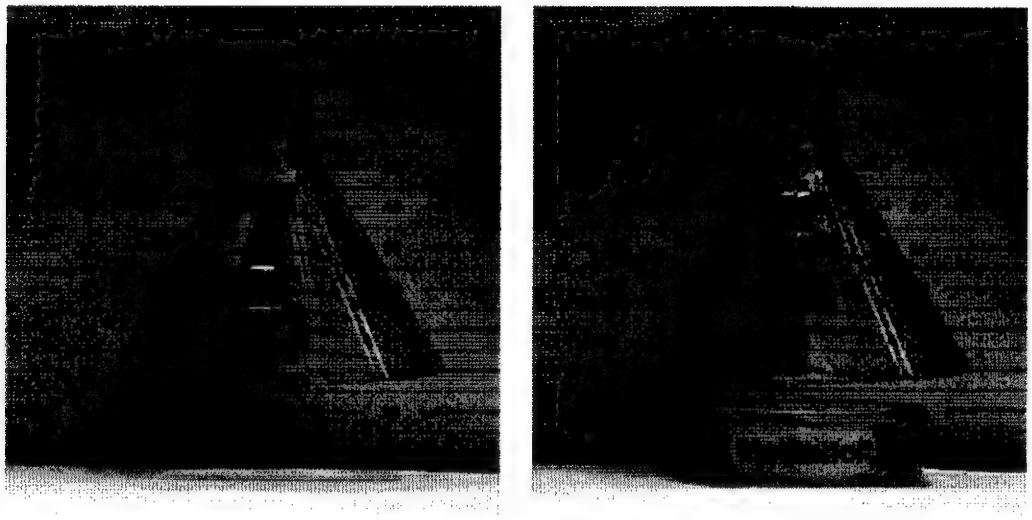

Figure 6. A Pt-coated nickel-titanium shape memory wire (top) contracts (right) upon exposure to a methanol/air mixture to lift a 50 g weight. This contraction raises the cylindrical plug in the inverted funnel, which cuts off the supply of methanol, thereby enabling the shape memory wire to elongate as a result of cooling. This cooling lowers the plug, thereby re-supplying the shape memory wire with fuel, and the actuation cycle repeats.

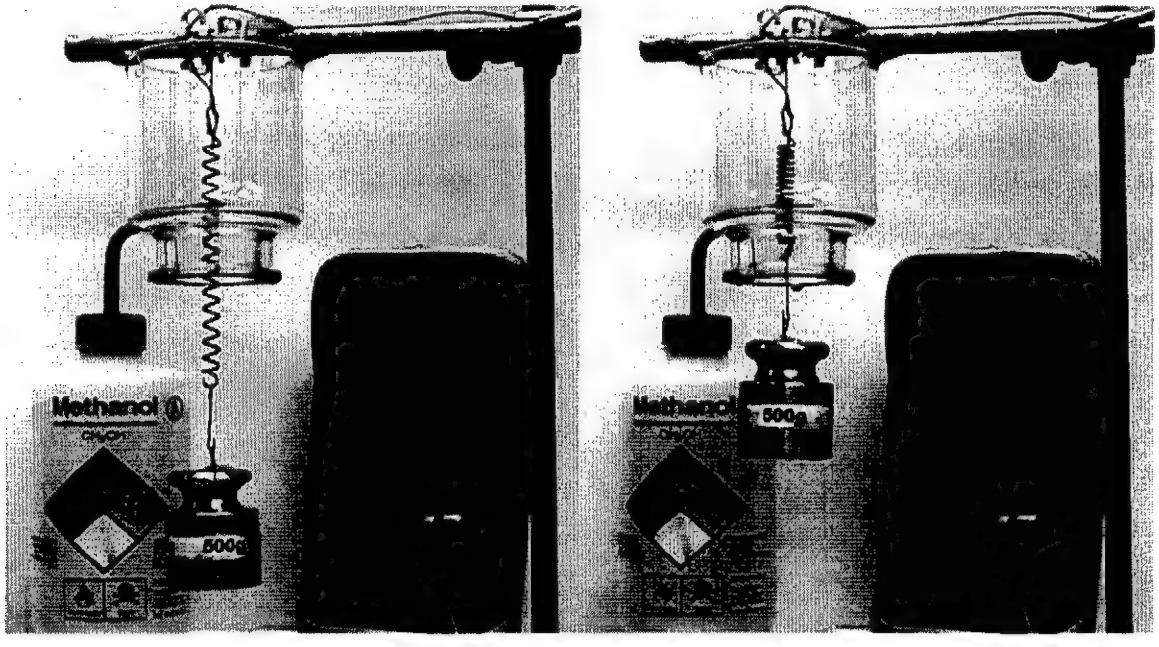

Figure 7. A Pt-coated NiTi shape memory spring lifts a 500 gram weight when exposed to a methanol/air mixture. The meter shows the temperature in °C that is measured at the top of the spring. The shape memory transition temperature is about 70 °C.

"Merged Concept" Fuel Powered Muscles

The properties of the two types of fuel-powered muscles can be merged to provide the benefits of both. In the "merged concept" muscle (Figure 8), the fuel (hydrogen) and oxidant are separated by a thin Nafion membrane (Nafion tubing) coated with Pt catalyst on inside and outside. The catalyst is in contact with an inner shape-memory-alloy (SMA) electrode (cathode) that can undergo shape-memory actuation upon fuel-generated electrical or thermal heating and the outer Pt electrode (wire anode) is wrapped around the Nafion tubing. These elements are enclosed in an outer plastic tube. Upon purging the inner tubing with 5% hydrogen in an inert gas and the outer tubing with oxygen, the device generates a voltage of about 0.9 V (Figure 9). On the anode side, hydrogen diffuses to the anode catalyst where it dissociates into protons and electrons. The protons are conducted through the membrane to the cathode, but the electrons are forced to travel in an external circuit because the membrane is electrically insulating. This electron transport in the external circuit causes electrical heating of the shape memory wire. On the cathode catalyst, oxygen molecules react with the electrons and protons to form water. The heat produced during fuel cell operation is sufficient to cause actuation of NiTi wire (though this actuation is presently much smaller than we obtain for actuation driven directly by fuel oxidation on the PT-coated surface of a shape-memory wire). The device can be controlled by hydrogen supply/interruption or shorting inner and outer electrodes.

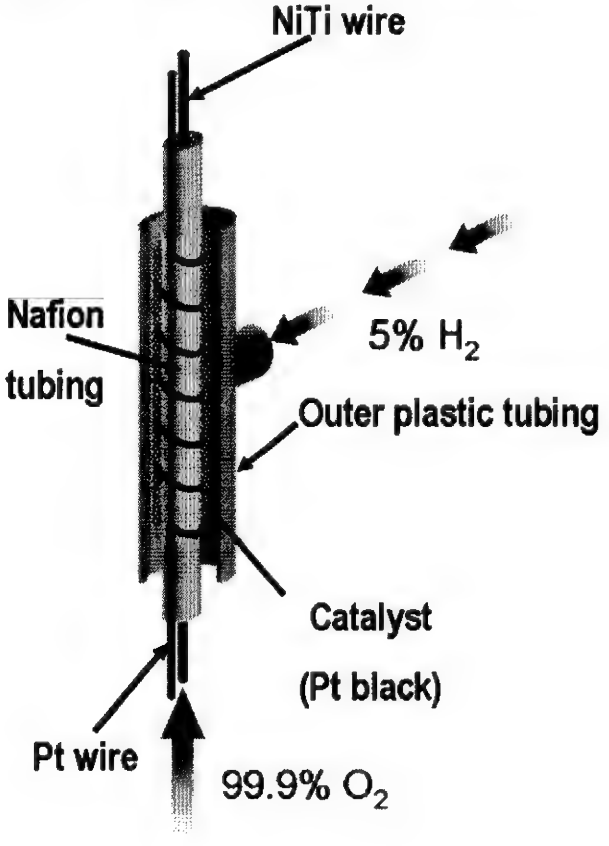

Figure 8. "Merged concept" muscle capable of generating electrical and mechanical power.

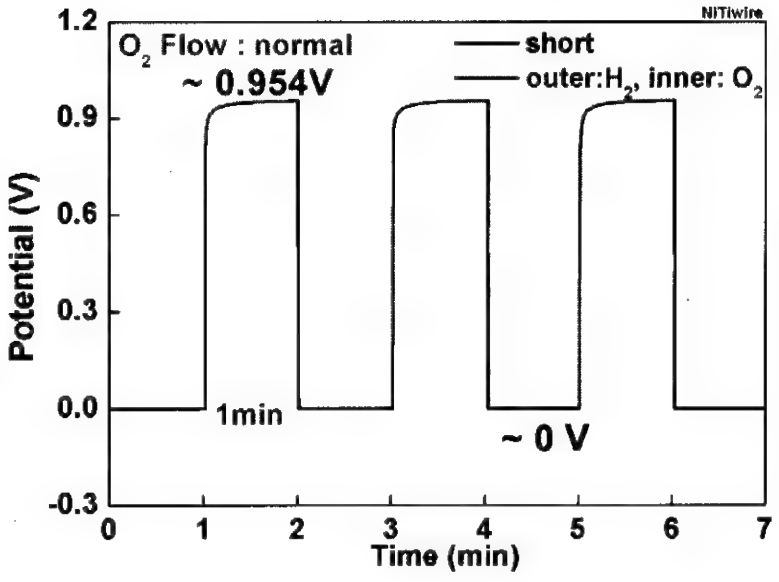

Figure 9. Voltage generation for device shown in Figure 8 upon fuel supply/interruption.

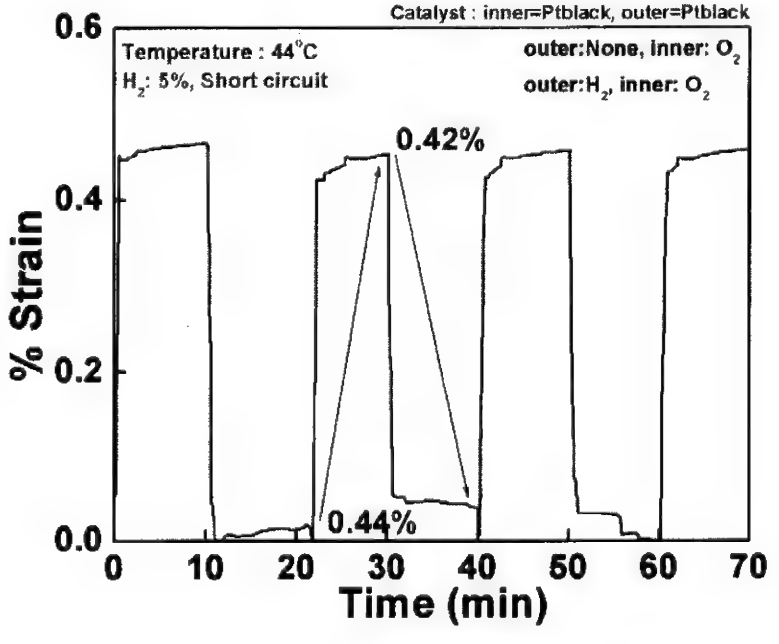

Figure 10. Strain generation by NiTi wire in device shown in Figure 8 upon fuel supply/interruption.

Electrochemical Actuation of Carbon Nanotube Yarns

The need for high performance artificial muscles motivated our development of twist based nanotube yarns and nanotube sheets, which we reported in two papers in *Science*. Actuation of the yarns in response to voltage ramps and potentiostatic pulses are presented below.

Individual carbon nanotubes (CNTs) offer exceptional properties. The tensile modulus of single walled carbon nanotubes (640 GPa) approaches that of diamond, while their tensile strength of approximately 20-40 GPa is about ten times higher than for continuous yarns or fibers of any type. Many research groups have been working to make bulk assemblies or yarns that can approach the modulus and tensile strength of individual CNTs. Interest in nanotube assemblies expanded in a new direction when we found that sheets of nanotubes (Bucky paper) actuate when used as an electrode in an electrochemical cell.[19] Since then actuation strains of up to 0.4 %[20] have been reported at effective strain rates of up to 19 %/s.[21]

Electrochemical double layer charge injection in the nanotubes causes actuation, via quantum mechanical and electrostatic effects that dominate for respectively small and large degrees of charge injection[19,22]. This double layer charge injection is a non-faradaic process in which changing the charge on the carbon atoms results in changes of C-C bond lengths[23,24]. The excess charge on the nanotubes is compensated at the nanotube-electrolyte interface by ions (cations or anions). The nanotubes act as double layer capacitors that are charged and discharged during actuation cycles.

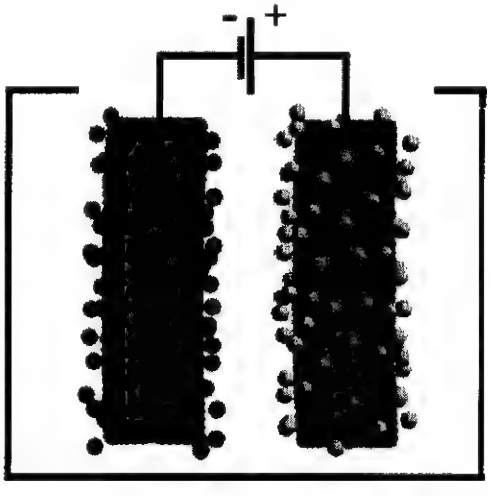

Figure 11 Ions of opposite charges are attracted to the CNT electrodes in an electrolyte when a voltage is applied, resulting in a change in the C-C bond length and actuation.

Because the Young's modulus of individual CNTs is extremely high, a relatively small strain of actuation will result in high stress generation, producing very high work densities per cycle. The actuation process can potentially be fast if charge can be injected quickly, leading to high power to mass ratios [21]. CNTs are stable at temperature as high as 1000°C if sealed from oxygen, making them appropriate for high-temperature actuation. However, before any of this can be realized it is necessary to make macroscopic structures out of CNTs that preserve the superb mechanical and electronic properties of the component CNTs. One approach is to spin fibers of aligned nanotubes. The present paper reports the first actuation measurements made on multiwall carbon nanotubes (MWNT) yarns that have been recently developed by the NanoTech Institute of the University of Texas at Dallas[25].

Methods

MWNT yarns were prepared by a dry spinning method [18], i.e., by drawing and twisting tubes from a forest. The MWNT forest was synthesized by catalytic CVD using acetylene gas as the carbon source. MWNTs, which are about 10 nm in diameter, are simultaneously drawn from the MWNT forest and twisted. The nanotube length in the forest is about 300 μm, resulting in yarn diameter between 1 and 60 μm, depending upon the forest width used for spinning. The twist is characterized by the helix angle (α), which depends directly upon the degree of twist and inversely on the yarn diameter. The degree of twist is typically 15000 turns/m.

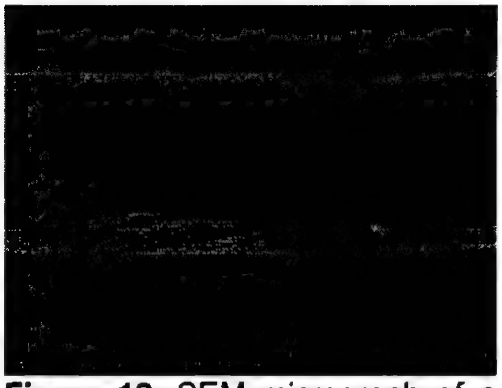

Figure 12. SEM micrograph of a twist-spun MWNT yarn.

In order to apply forces and record actuation forces and displacements generated by the CNT yarns, an Aurora Scientific ASI 300 muscle analyzer and its LabView-based software have been employed. Figure 13 is a photo of the apparatus used to apply force and of the yarn and clamping mechanism. The fiber is mounted between a lower fixed clamp and an upper movable motor arm. A computer-controlled potentiostat, similar to the one described in Ref.[25], is used to apply potentials. A data acquisition card (National Instruments 6036E) gathers the force and displacement data from the muscle analyzer and also logs the applied voltage and current.

For strain measurements in some experiments we employed Perkin-Elmer DMA 7e with a custom sample holder and electrochemical cell. The voltage was applied and current recorded via a Gamry Instruments potentiostat.

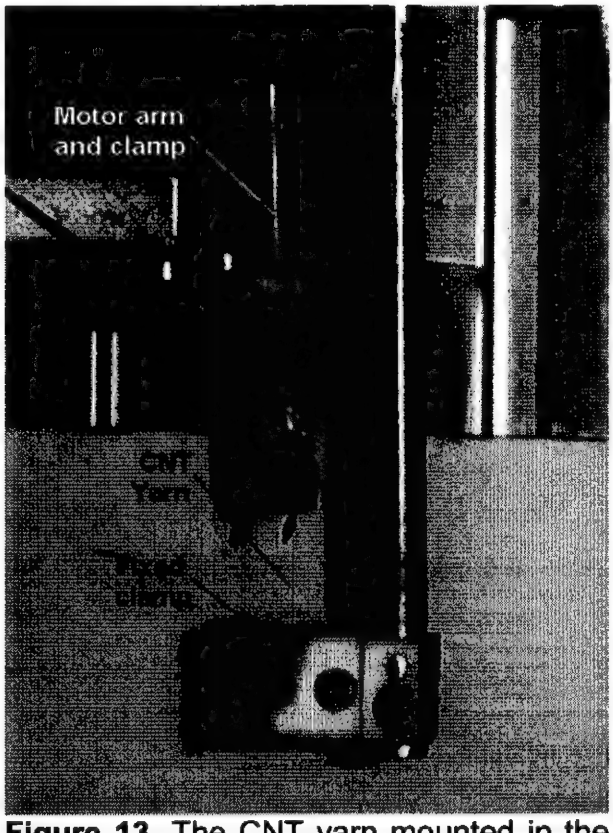

Figure 13. The CNT yarn mounted in the ASI muscle analyzer clamp.

Actuation

The electrolyte used is 0.2 M tetrabutylammonium hexafluorophosphate (TBAP) in acetonitrile (AN). A 12 mm length of single-ply yarn with a diameter of

18 μm was loaded to 11 MPa and was left in the electrolyte to relax for 30 minutes. Afterwards a triangular voltage input was applied at a scan rate of 500 mV/s, and the resulting currents and strains were measured. The reference electrode was aqueous Ag/AgCl and the counter electrode was a sheet of polypyrrole. The charge transferred (14d) was calculated by numerically integrating the current (14c).

The strain during cyclic voltametry (CV) is plotted versus nominal charge per C atom (including atoms on the interior of the tube) in Figure 15 for charging and discharging half-cycles with a quadratic fit for the charging half-cycle superimposed. The results match those obtained using carbon single walled nanotubes (SWNTs) [22] over the same range of nominal charge per atom. The

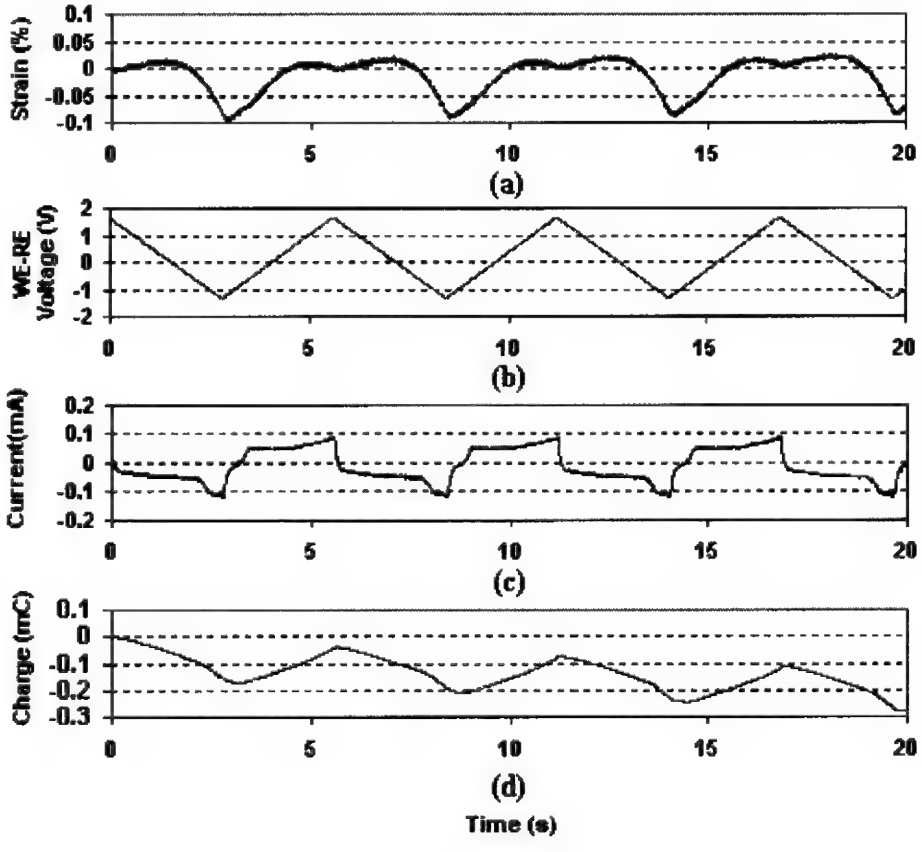

Figure 14. (a) Strain, (b) working electrode voltage, (c) cell current and (d) transferred charge during cyclic voltammetry of the MWNT yarn in 0.2 M TBAP in acetonitrile for an applied tensile load of 11 MPa.

similarity in actuation is consistent with the fact that the SWNT are bundled, since charge injection occurs non-uniformly in both cases – on the outer SWNTs in a SWNT bundle and the outer wall of MWNTs. Though the MWNTs are also bundled, the MWNTs are largely exterior to the bundle, where double layer charge injection can occur.The experiment was repeated at a scan rate of 100 mV/s. The resulting currents for 500 mV/s and 100 mV/s are plotted vs. the applied voltage (19a). The gravimetric capacitance of the yarn was estimated using the CVs to be 30 F/g over a potential range of –0.7 V to +0.7 V, as shown by the square response of an ideal capacitor in 16a. This high capacitance is very similar in magnitude to the capacitance observed in single wall carbon nanotubes [9], and is reasonable if the external surfaces of the MWNTs are largely accessible to electrolyte and the double layer capacitance of these nanotubes is 0.17 F/m^2. This result is derived from the measured capacitance and an estimate for the surface area per weight of MWNTs having an outer diameter of 10 nm and about 8 inner walls. It has been assumed that charge injection is only to outer walls and that all outer walls are accessible for charge injection.

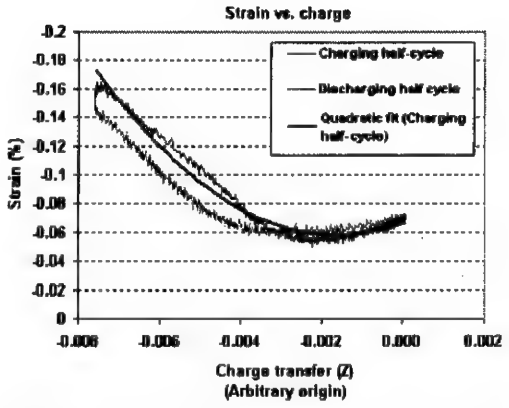

Figure 15 Strain vs. nominal charge per C atom during CV. The origin of the horizontal axis is arbitrary since the initial charge of the MWNTs is unknown.

A similar experiment was performed in 0.5 M tetrabutylammonium tetrafluoroborate (TBATFB) in acetonitrile (AN) again vs. Ag/Ag+ and with a Pt mesh/CNT counter electrode. The potential window was -2.5 to +2.5 V. The response to a triangular input scanned at 10 mV/s is shown in Figure 16b The voltammetry results suggest a capacitive response due to double layer charging of the nanotubes over a voltage range of approximately –0.7 V to +0.7 V vs. Ag/AgCl. The capacitance at 10 mV/s scan rate is estimated at 20-23 F/g, and implies a dependence of the capacitance on the scan rate. Beyond that range a kinetics-limited reaction is also contributing to the current. It may be the result of electrolyte degradation.

Figure 17 shows the actuation strain and the current in response to a series of voltage pulses with amplitudes between -2.5 V and +2.5 V. The electrolyte was 0.5 M TBATFB in AN. The maximum actuation strain achieved was measured to be 0.5 % using the Perkin-Elmer instrument described above. A similar experiment was performed using the ASI muscle analyzer. The voltages were applied using a Solartron SI 1287 electrochemical interface. The electrolyte was 0.2 M TBAP in AN, the reference electrode was aqueous Ag/Ag+ and the counter electrode was a sheet of polypyrrole. The pulses in each train had the same voltage amplitude. The experiment was repeated for voltage pulses relative to 0 V vs. Ag/Ag+ of -2.5V, -2V, -1.5V, -1V, -0.5V, 0V, 0.5V, 1 V and 2 V. Some

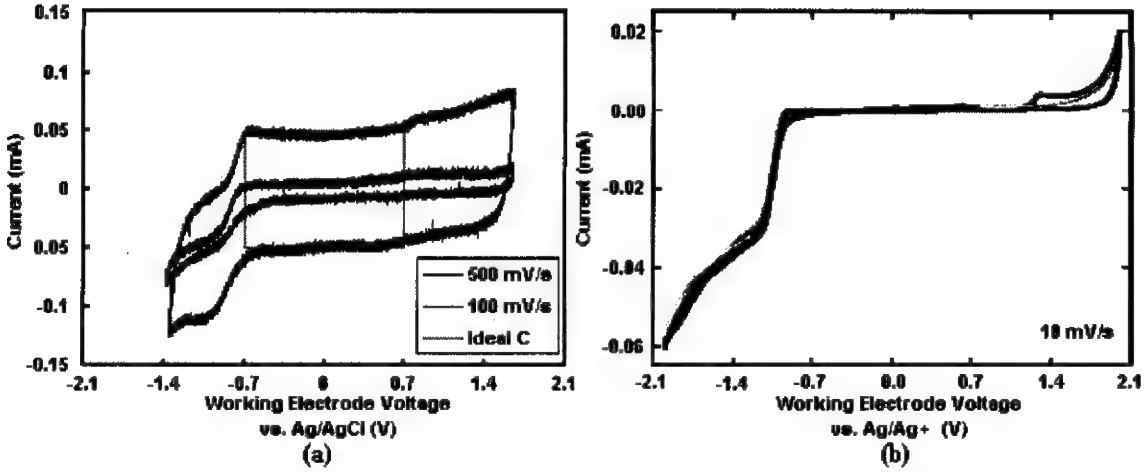

Figure 16. (a) Cyclic voltammogram for a 12mm-long single ply yarn at scanned at 500 and 100 mV/s. The rectangle shows the ideal capacitor response for a gravimetric capacitance of ~ 30 F/g at 500 mV/s. (b) CV of an 18 mm long yarn in 0.5 M tetrabutylammonium tetrafluoroborate (TBATFB) in acetonitrile (AN) at a scan rate of 10 mV/s

creep is observed during actuation. The creep seems to depend on the voltage amplitude, but the nature of this dependence has not yet been studied. The maximum strain achieved is 0.5 %

The amplitude of the resulting actuation strain is plotted vs. the applied voltage pulse amplitude in Figure 18. As the added trend line shows, the relationship is very close to a quadratic relationship, which is expected from previous results in single wall carbon nanotubes and theory[19,23,24]. This supports the suggestions that the forces producing strain are primarily coulombic in nature when the amount of charge injection is large.

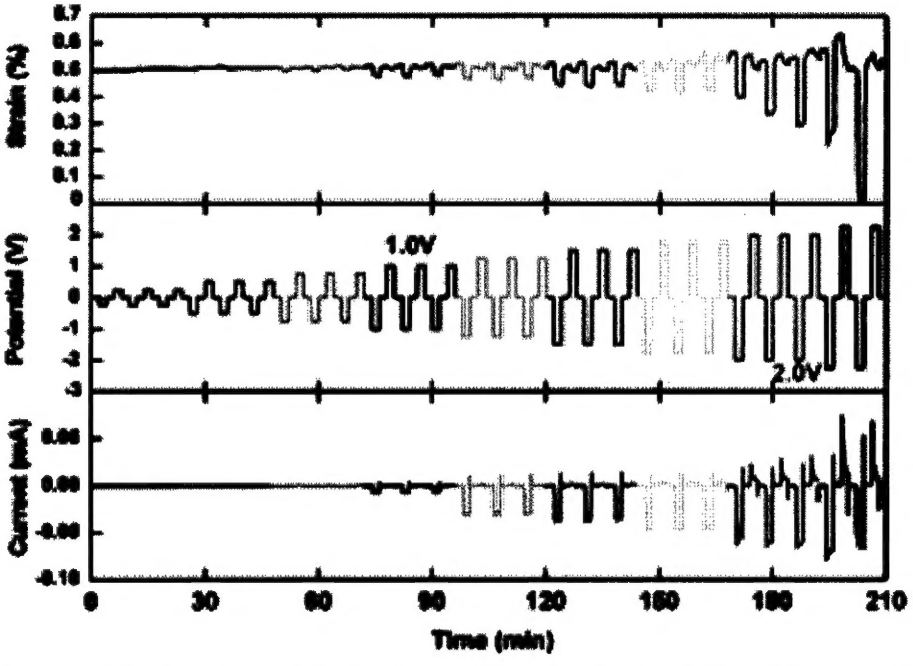

Figure 17. Applied voltage pulse trains vs. Ag/Ag+ and resulting actuation strains for actuation in 0.5 M TBATFB in AN

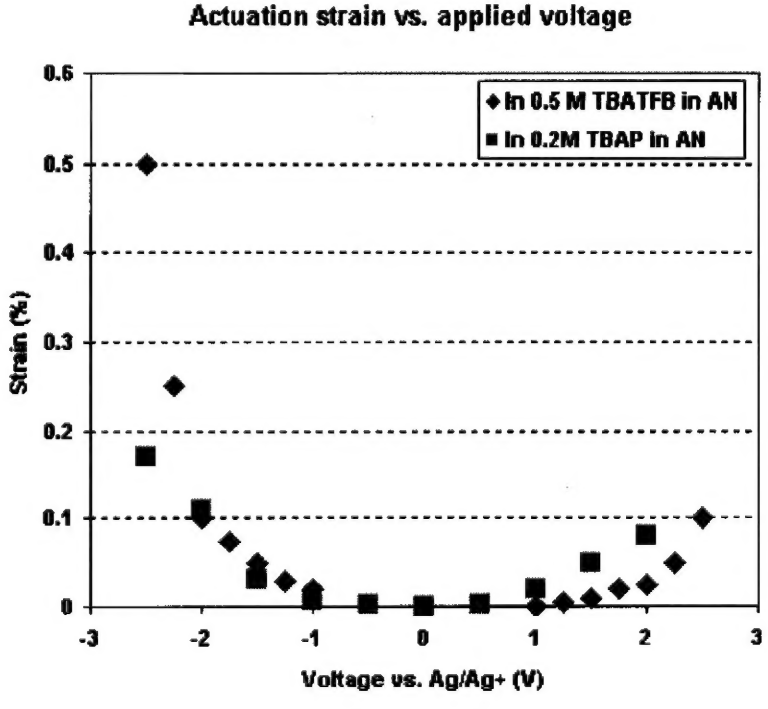

Figure 18. The strain amplitude plotted vs. the applied voltage amplitude.

The Young's modulus as a function of the oxidation state

The magnitude of isobaric actuation strain (i.e., for fixed load) can be influenced by potential- induced changes in modulus, as seen in polypyrrole [27]. The dependence of the Young's modulus on the charge state of the MWNTs was therefore studied.

The ASI 300 muscle analyzer was used to obtain stress/strain curves at a number of fixed potentials. The yarn was elongated by 0.1 % over a period of 0.5 s and then brought back to its original length. The applied strain waveform and the resulting stresses are plotted in Figure 19. Lines were fit to the resulting stress vs. strain curves for loading and unloading half-cycles. The relative slopes of these lines provide the effective Young's moduli of the yarn during loading and unloading.

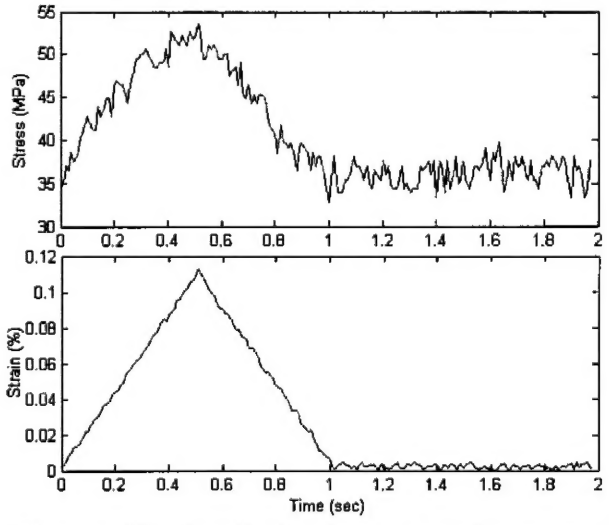

Figure 19. Applied strain waveform and the resulting stress to measure the Young's modulus of the yarns. The prestress was 35 MPa

No significant change in modulus is observed as the oxidation state is changed. The active strains are therefore not the results of static changes in the Young's modulus as a function of potential.

Summarizing this part of the program work effort, the yarns were found to actuate as a result of applied voltage. The actuation strain changes almost quadratically with applied voltage, as has been observed in single wall nanotubes, suggesting coulombic interactions as the primary mechanism of actuation. A maximum actuation strain of 0.5 % is reported at an applied voltage of -2.5 V. The gravimetric capacitance of the yarn is found to be approximately 30 F/g. The dependence of the tensile modulus on oxidation state has been studied and it is concluded that the Young's modulus is not strongly dependent on the oxidation state. Since modulus does not measurably change with charge injection, actuation strain should be insensitive to applied load.

PUBLICATIONS

1. M. Zhang, K. R. Atkinson, R. H. Baughman, Multifunctional Carbon Nanotube Yarns by Downsizing an Ancient Technology, *Science* **306**, 1358-1361 (2004).
2. R. H. Baughman, Playing Nature's Game with Artificial Muscles, *Science* **308**, 63-65 (2005).
3. M. Zhang, S. Fang, A. A. Zakhidov, S. B. Lee, A. E. Aliev, C. D. Williams, K. R. Atkinson, and R. H. Baughman, Strong, Transparent, Multifunctional Carbon Nanotube Sheets, *Science* **309**, 1215-1219 (2005).

4. V. H. Ebron, Z. Yang, D. J. Seyer, M. Kozlov, J. Oh, H. Xie, J. Razal, J. P. Ferraris, A. G. MacDiarmid, R. H. Baughman, Fuel Powered Artificial Muscles, *Science* **311**, 1580-1583 (2006).
5. D. W. Kim, J. S. Lee, G. S. Lee, L. Overzet, M. Kozlov, A. E. Aliev, Y. W. Park, D. J. Yang, Carbon Nanotubes Based Methanol Sensor for Fuel Cells Application, *J. Nanoscience and Nanotechnology*, **6**, 3608–3613 (2006).
6. T. Mirfakhrai, J. Oh, M. Kozlov, E. C. Wah Fok, M. Zhang, S. Fang, R. H. Baughman and J. D. W. Madden, Electrochemical actuation of carbon nanotube yarns, *J. Smart Materials and Structures*, 2006, submitted.
7. M. Zhang, K. R. Atkinson, R. H. Baughman, Multifunctional Carbon Nanotube Yarns and Sheets, PCT patent application.
8. M. E. Kozlov, R. C. Capps, V. H. Ebron, J. P. Ferraris, R. H. Baughman, Polymer Free Carbon Nanotube Assemblies (Fibers, Ropes, Ribbons, Films), PCT patent application.
9. V. B. Ebron, Z. Yang, D. J. Seyer, M. Kozlov, J. Oh, H. Xie, J. Razal, J. P, Ferraris, A. G. MacDiarmid, R. H. Baughman, Fuel Powered Artificial Muscles, Provisional Patent Filing.

References

1. J. D. W. Madden, N. A. Vandesteeg, P. A. Anquetil, P. G. A. Madden, A. Takshi, R. Z. Pytel, S. R. Lafontaine, P. A. Wieringa, I. W. Hunter, *IEEE J. OCEANIC ENGINEERING* **2004**, *29*, 706.
2. R. H. Baughman, *Science* **2005,** *308*, 63.
3. E. Smela, *Advanced Materials* **2003**, *15*, 481.
4. R. Pelrine, R. Kornbluh, Q. Pei, J. Joseph, *Science* **2000**, *87*, 836.
5. Q. M. Zhang, V. Bharti, X. Zhou, *Science* **1998**, *210*, 2101.
6. S. Nemat-Nasser, Y. Wu, *J. Appl. Phys.* **2003**, *93*, 5255.
7. J. Weissmüller, R. N. Viswanath, D. Kramer, P. Zimmer, R. Würschum, H. Gleiter, *Science* **2003**, *300*, 312.
8. S. Hara, T. Zama, W. Takashima, K. Kaneto, *J. Mater. Chem.* **2004**, *14*, 1516.
9. H. B. Schreyer, N. Gebhart, K. J. Kim, M. Shahinpoor, *Biomolecules* **2000**, *1*, 642.
10. R. H. Baughman, C. Cui, J. Su, Z. Iqbal, A. A. Zakhidov, US patent 6,555, 945, April 29, 2003.
11. J. H. Robert, US Appl. Pub. No. 0028901 Feb 10, 2005.
12. Dao Min Zhou, US Appl. Pub. No. 0192784 Oct 16, 2003.
13. T. Hirai, J. Zheng, M. Watanabe, H. Shirai, *Smart Fibers, Fabrics and Clothing*, **2001**, 7-33.
14. Y. Osada, H. Okuzaki, H. Hori *Nature*, **1992**, *355*, 242.
15. T. Tanaka, I. Nishio; S. Sun; S. Ueno-Nishio *Science*, **1982**, *218*, 467.
16. R. H. Baughman, *Synthetic Metals* **1996**, *78*, 339.
17. J. Ping Gong, Y. Katsuyama, T. Kurokawa, Y. Osada, *Adv. Mater.,* **2003**, *15*, 1155.

18. M. Zhang, K. Atkinson, R. H. Baughman, *Science,* **2004**, 306, 1358.
19. R. H. Baughman, C. Cui, A. A. Zakhidov, Z. Iqbal, J. N. Barisci, G. M. Spinks G. G. Wallace, A. Mazzoldi, D. De Rossi, A. G. Rinzler, O. Jaschinski, S. Roth M. Kertesz, *Science,* **1999**, *284,* 1340.
20. J. N. Barisci, G. M. Spinks, G. G. Wallace, J. D. Madden, R. H. Baughman *Smart Mater. Struct.* **2003**, *12,* 549.
21. J. D. W. Madden, J. N. Barisci, P. A. Anquetil, G. M. Spinks, G. G. Wallace, R. H. Baughman, I. W. Hunter, *Advanced Materials,* **2006**, *18,* 870.
22. G. M. Spinks, G. G. Wallace, R. H. Baughman, L. Dai, in *Electroactive Polymers (EAP) Actuators as Artificial Muscles, Reality, Potential and Challenges*, ed Y Bar-Cohen, (Bellingham WA: SPIE press) **2004**, 261.
23. C. T. Chan, W. A. Kamitakahara, K. M. Ho, P. C. Eklund, *Phys. Rev. Lett.* **1987**, *58,* 1528.
24. L. Pietronero, S. Strässler, *Phys. Rev. Lett.* **1981**, *47,* 593.
25. J. D. Madden, R. A. Cush, T. S. Kanigan, I. W. Hunter, *Synthetic Metals* **2000**, *113* 185.
26. J. N. Barisci, G. G. Wallace, D. Chattopadhyay, F. Papadimitrakopoulos, R. H. Baughman, *Journal of the Electrochemical Society* **2003**,*150*, E409.
27. G. M. Spinks, L. Liu, G. G. Wallace, D. Zhou, *Advanced Functional Materials* **2002**, *12* 437.